Switching hydrodynamics in liquid crystal devices: a simulation perspective

Soft Matter

REVIEW

View Article Online
View Journal | View Issue

Cite this: *Soft Matter*, 2014, **10**, 4580

Switching hydrodynamics in liquid crystal devices: a simulation perspective

A. Tiribocchi,[a] O. Henrich,[b] J. S. Lintuvuori[a] and D. Marenduzzo*[a]

Received 8th January 2014
Accepted 31st March 2014

DOI: 10.1039/c4sm00042k

www.rsc.org/softmatter

In liquid crystal devices it is important to understand the physics underlying their switching between different states, which is usually achieved by applying or removing an electric field. Flow is known to be a key determinant of the timescales and pathways of the switching kinetics. Incorporating hydrodynamic effects into theories for liquid crystal devices is therefore important; however this is also highly non-trivial, and typically requires the use of accurate numerical methods. Here, we review some recent advances in our theoretical understanding of the dynamics of switching in liquid crystal devices, mainly gained through computer simulations. These results, as we shall show, uncover interesting new physics, and may be important for future applications.

1 Introduction

Liquid crystals (LCs) are prime examples of soft materials in which long-range order correlations are combined with fluidity.[1] LC displays (LCDs)[2,3] represent one of the most successful and widespread applications, and today they dominate the display device market. The high interest in studying LCs is also due to applications beyond display devices,[4] such as LC elastomers,[5] colloid–LC composites for use as photonic crystals,[6] LC creams,[7] and even liquid crystalline food.[8] The framework of LC theory has also proved useful to describe biological matter,[9] such as dense suspensions of swimmers,[10] cell cytoskeleton and membranes[11] as well as bird flocks.[12]

In this review we discuss the physics behind the switching of LC devices, focussing on the effects of hydrodynamics and flow, based on results obtained from computer simulations, which are necessary in view of the intricacy of the underlying equations of motion. We consider devices which are either based on nematic LCs or on blue phases as these are important representatives of both present day commercially successful LC devices and their potential future development. It was during the late 1970s and the early 1980s that the combination of increasing popularity of liquid crystals as a research field and rapid development of industrial manufacturing technologies led to the construction of the first twisted nematic (TN)[13] and super-TN cells.[14] Since then the scientific community has always remained engaged in research that is motivated by the construction of liquid crystal devices. This has gone hand-in-

[a]*SUPA, School of Physics and Astronomy, University of Edinburgh, Mayfield Road, Edinburgh, EH9 3JZ, UK. E-mail: dmarendu@ph.ed.ac.uk*

[b]*EPCC, School of Physics and Astronomy, University of Edinburgh, Mayfield Road, Edinburgh, EH9 3JZ, UK*

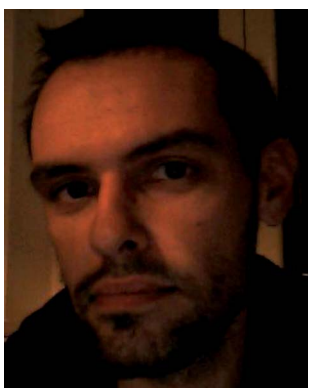

Adriano Tiribocchi is a Postdoctoral Research Associate in the School of Physics and Astronomy at the University of Edinburgh. He studied at the Department of Physics of Bari (Italy) where he received his PhD in theoretical physics in 2011. He worked on lattice Boltzmann simulations of liquid crystals and binary fluids. His current research interests include simulations of active liquid crystals and field theories for active matter.

Oliver Henrich is an Advanced Fellow at the Edinburgh Parallel Computing Centre. This was preceded by postdoctoral appointments at the Centre for Computational Science, University College London and at the School of Physics and Astronomy, the University of Edinburgh. His current research interests include rheology and structure of liquid crystals, flow of charged soft condensed matter, the lattice Boltzmann method and high performance computing.

hand with the development of innovative applications, such as the thin-film transistor technology developed in the late 1980s, followed by notebooks and culminating in the large and small display technology that currently occupies a vast segment of the market of mobile phones and monitors. Several features make LCDs particularly attractive compared to other display technologies, the most important ones being their compactness and portability, thinness and low production costs. These factors render them suitable for large sized (more than 24 inches), light and relatively inexpensive displays. On the other hand there are some important and classic drawbacks which affect the functionality of liquid crystal displays, and resolving these issues remains a constant focus of attention from a technological point of view. The main limitations are related to the "viewing angle" problem and the relatively high power consumption (although lower than most of the other display technologies).

As we shall see in this review, gaining a deeper understanding of the physics of liquid crystal devices allowed some of these problems to be addressed and at least partially solved. Particularly in the field of devices scientific and technological breakthroughs are intimately coupled and theory and experiments need to proceed at the same pace. Often a specific application raises a challenging problem, which is then tackled by theory. Also the reverse sequence can occur, for instance the huge potential of devices based on blue phases has already been explored in theory, but has not been fully realised in practical applications. As anticipated, our focus in this review is on the theory behind the switching dynamics of liquid crystal devices and particularly on the role of hydrodynamics and flow. The results are mostly gained through computer simulations, which have proved to be extremely useful to complement theoretical and experimental studies of liquid crystal devices.[15–19] Computer simulations have been so useful because in the theoretical framework flow and order parameter fields are intimately coupled in a strongly non-linear way. This defies most analytical attempts to describe the switching. Furthermore, the geometries and boundary conditions used in real device designs are also often highly non-trivial, and simulations are uniquely suited to describe them accurately.

The organisation of this review is as follows: we will first discuss devices based on nematics (Section 2), followed by blue phase based designs (Section 3). Section 4 concludes with a brief discussion. We would like to point out that here we concentrate on the results and their relevance to the physics of liquid crystal device switching, for this reason we give only a brief description of the standard equations of motion for liquid crystal hydrodynamics in Appendix A. The interested reader who wishes to know more about the methodology should refer to ref. 20 and 21 or the original papers reviewed herein.

2 Nematic based devices

In nematic LCs the molecules adopt a state where they align on average along a preferred direction. This is described by a unit vector with head–tail symmetry, also referred to as director field **n**. It is important to highlight that in nematics, as in most liquid crystalline phases, there is only long-range orientational order and no positional order between its building blocks, rod-like or disc-like shaped molecules. The orientational order is responsible for the macroscopic anisotropy of LCs, which is arguably the most prominent property that finds use in technological applications.[1]

Nematics form currently the widest class of LCs used for the construction of flat panel monitors and more generally any LC based display. A typical twisted nematic (TN) device (still the most commonly used technology) consists of two transparent electrodes placed at a distance of a few micrometers from each other, and of two crossed polarising filters in which the LC is embedded. The equilibrium zero-field state of the director is characterised by a helical arrangement determined by the surface alignment of the LC molecules (normally a conflicting homogeneous, or planar, anchoring, see Fig. 1a).

This setup induces a rotation of the polarisation plane of the incident light, which allows the light to pass through the second polariser leaving the pixel white. When an electric field is applied, and for a positive dielectric constant, the molecules in the centre of the device align along the field direction. The polarisation of incident light will be therefore perpendicular to the second filter and hence the pixel will appear black.

Juho Lintuvuori is a Postdoctoral Research Associate in the School of Physics and Astronomy at the University of Edinburgh. He received his PhD from the University of Durham in 2010, where he studied self-assembling molecular materials using coarse grained modelling. His current research interests include the coupling between flow and order in driven complex fluids including liquid crystals and colloidal solutions.

Davide Marenduzzo is a Reader in Biophysics at the University of Edinburgh. He received his PhD from the International School for Advanced Studies (SISSA/ISAS, Trieste, Italy) in 2002. His main research interests currently include liquid crystals, active matter, and biophysics (especially the physics of DNA and chromosomes).

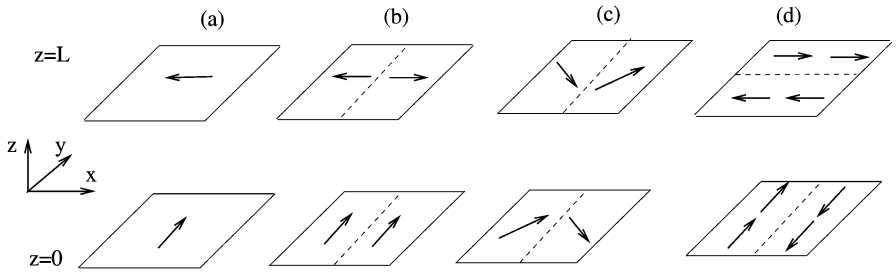

Fig. 1 Anchoring geometry of the director profile on the surfaces of several devices: (a) single domain (b and c) two-domain and (d) four-domain TN device. Reproduced with permission from ref. 15.

Conversely, when the electric field is switched off, the director field regains the twisted structure favoured by the boundaries, and the pixel turns white.

The switching off, or relaxation time, τ_{off}, may be estimated in terms of the physical parameters characterising the liquid crystals (see the Appendix for more thorough discussion of the equations of motion where such quantities appear) as

$$\tau_{off} \sim \frac{\gamma_1 L^2}{K} \quad (1)$$

where γ_1 is the rotational viscosity of the liquid crystal (measuring the resistance to director rotation, and typically 0.1–1 poise), L is the length scale, which for a twisted nematic cell equals the device size (typically in the micron range), and K is the average elastic constant of the liquid crystals (or a suitable combination of the splay, bend and twist elastic constants, typically $\sim$10 pN). We note that the timescale in eqn (1) (which is typically $\sim$1 or more ms in reality[22]) can be obtained essentially on dimensional grounds, and is indeed a classical timescale in liquid crystal dynamics, and it is the one associated with the reorientation of the director field.[1]

On the other hand, the dynamics of the switching off is controlled by the magnitude of the field, and, up to a multiplicative constant, the switching on time, τ_{on}, can be estimated as (see *e.g.* ref. 22 and references therein)

$$\tau_{on} \propto \frac{\gamma_1 L^2}{\varepsilon_a \left(V^2 - V_{thr}{}^2\right)} \quad (2)$$

where ε_a is the dielectric anisotropy of the liquid crystal (see Appendix), V is the applied voltage (typically 1–100 V in micron-sized devices), and V_{thr} is the critical voltage below which the device does not switch on. For large V, then, $\tau_{on} \sim \gamma_1 L^2/(\varepsilon_a V^2)$, which can again be obtained by dimensional analysis, in cases where the dynamics is dependent on the voltage, as during switching on.

Although easy to be built in practice, the twisted nematic device suffers from several drawbacks as previously mentioned. The most important one is the "viewing angle problem",[23] which refers to the limited maximum angle from which an image is clearly visible on the display. The energy consumption is also relatively large, mainly due to the necessity to have the electric field continuously on during operation of the device.[16] The first of these shortcomings can be partially solved with the so-called "multi-domain" technology (see Fig. 1), which was proposed in the late 1980s. A patterned anchoring of the LC on the surfaces creates regions of left and right-handed twists in the cell. These domains have different viewing angle limitations, hence their simultaneous presence in one single device leads to an overall less stringent restriction. However, the topological defects or disclinations that emerge now naturally between regions with different orientations are generally responsible for the loss of resolution.

On the other hand, bistability, or multistability, can provide a route towards the next generation of devices with improved energy efficiency. In a bistable (or multistable) device, a liquid crystal can be sequentially switched by a field into two (or more) metastable states. In all cases the metastable state is retained after the field is switched off. Devices like these are technologically very attractive as they can operate without constant application of an electric field. This allows a significant decrease in energy consumption together with a dramatic reduction of the amount of electronic circuits required, with advantageous consequences for weight and portability. A well-known example of an experimentally realised nematic multistable device is the zenithal bistable device,[17–19] whose bistability relies on flexoelectricity combined with a periodic grated structure of the surfaces. Another example is the device proposed in ref. 25, in which a hexagonal multi-domain tiling of the molecules on one or both surfaces creates three stable macroscopic orientations of the LC that are mutually switchable by an in-plane electric field. In addition, a bistable device has been proposed in ref. 16 in which a two-domain hybrid aligned nematic (HAN) cell provides a remarkably simple route to achieve bistability. In most of these cases, though, several of the metastable states involve again topological defects or disclinations.

The physics of multistable devices is therefore crucially linked to the detailed understanding of the defect structure and of their dynamics under an external field. For example one is interested in answering the following questions. What is the defect structure corresponding to the zero-field case? What is the role played by the defects during the switching? How do hydrodynamic interactions affect the switching dynamics? To properly address these key questions, modelling and simulation are of fundamental importance. Here, we review recent results, published in ref. 15 and 16, concerning simulations of switching hydrodynamics of nematic LCs confined in cells whose geometry is inspired by the design of a real device. Another

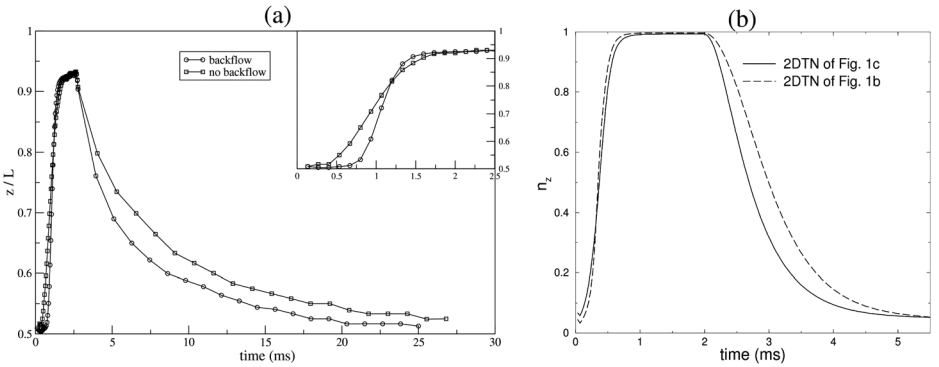

Fig. 2 (a) Time evolution of the z position of the disclination with and without backflow. The inset is an enlargement of the switching on dynamics. (b) Time evolution of the z component of the director field along z for the two devices as in Fig. 1b and c. Reproduced with permission from ref. 15 where also all the parameters are defined.

related numerical investigation of dynamics in a device geometry was presented in ref. 24.

The first geometry we describe is depicted in Fig. 1b. It consists of a two-domain structure in which left- and right-handed stripes of nematic LCs are separated by a twisted disclination line that lies parallel to the y-axis and is located at the centre of the cell. Boundaries are in the xy-plane where the director is homogeneously anchored (this can be obtained experimentally by rubbing the surface); here and in what follows it is assumed that light travels along the z direction, perpendicular to the planes, while the distance between the planes in the simulated device is in the micron range, as in reality. The system is periodic along the x- and y-directions. Fig. 2a shows a plot of the z-position of the defect as an electric field is applied perpendicular to the walls and is then switched off. When the field is switched on, the defect moves towards the top wall and gets pinned to the surface, whereas the defect finds its way back to the centre of the cell when the field is switched off. This means that the cell is electrically *switchable*, or in other words, one can cycle between a field-induced "on" state and a field-free "off" state. Switchability is clearly a key property for any device with potential technological applications. In the next section we will show that this property is also shared with devices based on cholesteric blue phase LCs.

Interestingly, the switching-off dynamics is much slower than the switching-on process. This is because the driving force, the difference in free energies between the zero-field and the field-induced state, is small. In this case, indeed, as in other cases where there is a transition between two different states, with difference in free energy density equal to Δf, one expects τ_{off} to be directly proportional to γ_1 and inversely proportional to Δf (see *e.g.* ref. 26 where the velocity of the disclination in a cholesteric device was shown to scale in a way consistent with this argument). In addition, backflow† (Fig. 2a with circles) leads to a delay in the onset of the switching on and reduces the relaxation times significantly when the field is removed. This behaviour seems to be quite generic, given that it has also been observed in BPI and BPII devices,[27] where a similar dynamic protocol for the electric field has been adopted. On the other hand, the time it takes for the defect to get back to the centre of the cell is still longer than for a conventional TN device. A possible technological solution could be to stabilise the domain structure with a surface $\pi/2$ pre-twist (see Fig. 1c). This is explicitly shown in Fig. 2b, where the evolution of the z-component of the director field is plotted for both two-domain devices.

We note that experimental realisations of multi-domain devices such as those treated in ref. 15 were explored prior to the theory, in view of their potential use to solve the viewing angle problem. One of these devices was built in ref. 28 in terms of a four-domain tiling of the director on the surfaces, which allows the formation of stripes of two left-handed and two right-handed twist regions organised in a checkerboard-like pattern (see Fig. 1d). This design gives rise to a complicated defect structure whose switching dynamics has been discussed in ref. 15.

Another example of a multi-domain device has been studied in ref. 16: this is a two-domain HAN cell (whose geometry is shown in Fig. 3a), and it provides an interesting example of a bistable device.

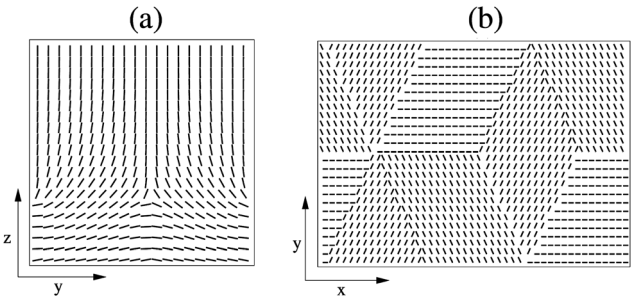

Fig. 3 (a) Two-domain cell with homeotropic anchoring at the top and homogeneous anchoring with a pre-tilt pattern of ~10° at the bottom. (b) Surface patterning used for the top and bottom walls of the 3-domain tristable device of ref. 25. Reproduced from ref. 16. Copyright American Institute of Physics (AIP).

† Hydrodynamic interactions in liquid crystals are often referred to as *backflow*, which generally denotes the coupling between velocity field and director orientation.

The initial zero-field two-domain structure in Fig. 3 is due to the mixed anchoring conditions of the director on the surfaces with homeotropic (or perpendicular) on one wall and homogeneous (or parallel) on the opposite wall. A small pre-tilt of about 10° stabilises a defect of −1/2 topological charge in the bulk of the cell (Fig. 4a). The presence of domains with homeotropic and homogeneous anchoring in one single setup stimulates the emergence of a predominantly homeotropic or homogenous domains (Fig. 4a) and makes bistable behaviour possible. The dynamical protocol of the applied electric field is rather simple: when the field is applied along the *y*-direction the defect annihilates and, after the field has been switched off, the director gets stuck in a one-domain structure with low free energy (see Fig. 4b). This can be fully reverted by applying a sufficiently strong pulse along the *z*-direction, which results in the device recovering the previous two-domain structure with the same free-energy (Fig. 4c). Backflow (hydrodynamics) reduces the likelihood to observe bistability, mainly because it drives the system towards states that have similar free energies.

The idea of using the multidomain technology as a route to achieve multistability in devices has been applied with enormous success. An example is a tristable device proposed in ref. 25. The typical director pattern on the surfaces is shown in Fig. 3b. This surface anchoring templates a metastable initial defect network in the bulk, in which column disclinations of integer and half-integer topological charge are oriented perpendicular to the walls and span the whole device. The dynamics of these disclination lines in an electric field have been discussed in ref. 16, and are characterised by a complex reshaping of the director field pattern. This leads to the formation of transient disclination loops which reconstruct into an array parallel to the wall and pinned to the surfaces (see Fig. 3 in ref. 16). Eventually, after the field has been applied and removed along one of the directions of the surface patterning, surface defects appear and the bulk of the liquid crystal remains nematically aligned along the field direction (these resulting patterns are the multistable states).

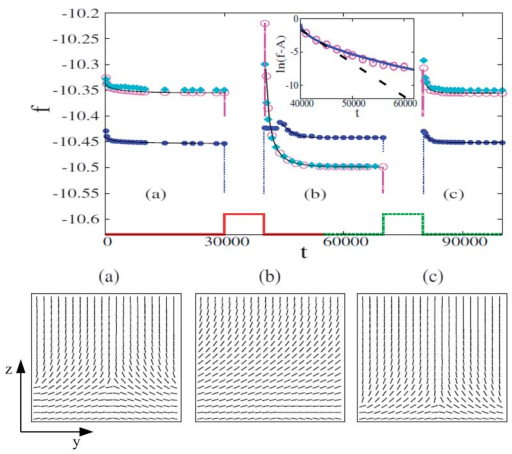

Fig. 4 Free energy evolution (top panel) of the HAN cell. Filled squares correspond to a simulation with backflow. The step function is non-zero when the field is applied. The director profile of the equilibrium zero-field states is shown in the bottom panel. When an electric field is applied along the *y*-direction (switched on at $t = 30\,000$ and off at $t = 40\,000$), the system relaxes to a stable state ((b) in the bottom panel, snapshot at $t = 70\,000$), but in a different minimum free energy. Then an electric field is applied along the *z*-direction at $t = 70\,000$ and is switched off again at $t = 80\,000$. The relaxation process drives the system back to state (a). The relaxation curves for the two cases without backflow (open and filled circles) were fitted with a stretched exponential and the inset shows a comparison with a simple exponential (dashed line). Reproduced from ref. 16. Copyright American Institute of Physics (AIP).

It is worth mentioning that all switching mechanisms described above involve LCs whose building blocks are rod-like shaped. It is appropriate to assume that the orientational order parameter couples quadratically to the electric field (this is the so-called *dielectric coupling*, see Appendix). Depending on the sign of the dielectric anisotropy the molecules tend to align them either parallel or perpendicular to the field. Different classes of LCs consisting of pear- or banana-shaped molecules[1] can instead show spontaneous polarisation in the presence of an elastic distortion. The opposite effect, an elastic distortion generated by polarisation that is induced by an electric field, is also possible. The coupling between the variation of the orientation and the external field is called *flexoelectric coupling* and is linear in the applied field (see Appendix). This behaviour makes it dominant over the dielectric coupling for low enough voltages; the classical example of a device which exploits the physics of flexoelectricity is the above mentioned zenithal bistable device.[17–19]

Another emerging class of LC devices is based on the idea of switching the LC *via* microfluidic *flow* rather than by external electric fields. While integrated devices that combine microfluidics and optics have received a lot of attention during the last decade, devices that use LCs are still almost unknown. In ref. 29 a device is presented that translates a periodic volume modulation into a modulated optical retardation and transmission in a microfluidic cell. The top picture in Fig. 5 shows the basic operating principle. A needle is connected to a reservoir holding a nematic liquid crystal which is itself connected to a microchannel. Up and down movement of the needle together with homeotropic anchoring conditions at the wall of the channel cause the LC to buckle and undergo changes in the order parameter structure. This novel way of operating a LC device by flow offers a number of advantages over conventional switching mechanisms, such as fast and symmetric response in the submillisecond range, a regime which is out of reach for most conventional devices based on nematogens. At the same time it makes use of the advanced and sophisticated alignment control that we have gained to date over nematic LCs. The bottom picture of Fig. 5 shows a few cycles at a relatively moderate frequency of 178 Hz and the symmetric response times.

The construction microfluidic devices based on LC media may be still at an early stage. However, it seems interesting to ask how the defect structure influences the flow behaviour, a link that could be used for a variety of other switching mechanisms. In ref. 30 and 31 the bulk switching behaviour of blue phases in a simple shear flow has been studied. This revealed a complex flow behaviour that depends directly on the topology of the disclination network and the ratio of viscous to elastic

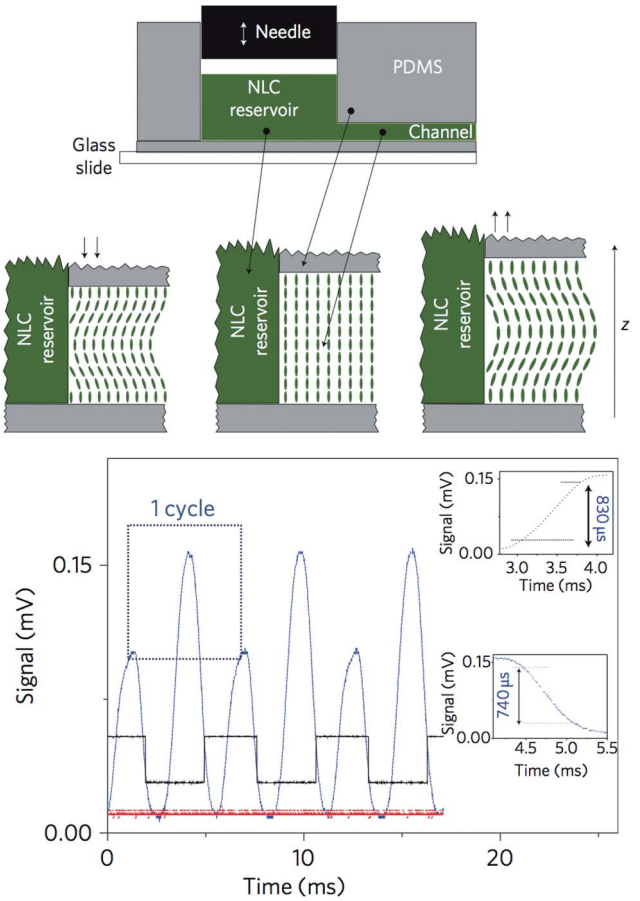

Fig. 5 Peristaltic flow of nematogens in microfluidic channels: the top picture demonstrates the basic principle and the effect of the peristaltic flow on the alignment of the nematic liquid crystal. The bottom picture shows the transmission signal for the steady state (red) and periodic modulation (peristalsis) (blue) together with the driving pulse (black). Light travels along the vertical direction; crossed polarising filters are placed on opposite parts of the cell. The insets give magnifications of the on and off profiles. Reproduced from ref. 29. Copyright Nature Publishing Group.

forces, which is quantified in the dimensionless Ericksen number. A similar computational study may shed a lot of light on the dynamics of the "optofluidic" device of ref. 29.

3 Cholesteric and blue phase based devices

As is clear from the results reviewed in the previous section, understanding the defect dynamics and how it is affected by hydrodynamics or by an external electric field is therefore crucial to capture the physics of many nematic liquid crystal devices, as well as to improve their performance. This is even more important in devices based on cholesteric and blue phases, to which we turn in this section, as in these systems the disclination network has a more intricate structure.

In cholesteric or chiral nematic liquid crystals (ChLCs), the director field **n** features a twist deformation in the direction perpendicular to the symmetry axis of the molecules, whereas in blue phases the director field twists along more than one direction. The periodicity in the twist deformation introduces another length scale, the pitch, p, which is of the order of microns or larger, for cholesterics, while it lies in the hundreds of nanometer range for blue phases. This additional length scale may substitute the device size L in our estimates the switching times τ_{on} and τ_{off} (see eqn (2) and (1)): particularly in the case of blue phases, even the switching off times may easily be in the sub-millisecond range, which renders these materials very attractive for devices. While most ChLCs used in display devices[32] are man-made, and can be obtained by adding a chiral dopant to a nematic LC, a naturally occurring instance of ChLCs is DNA in solution at low or moderate concentrations.

Because of their special optical properties, first and foremost their periodic refractive index as a result of the local director twist, ChLCs have been used in several applications ranging from temperature sensors to displays, such as polymer stabilised surface textures. Focal conic defects stabilised at zero electric field can be switched into the homeotropic texture (also known as the "fingerprint" texture, where the direction of the cholesteric helix is parallel to the boundary planes) when an electric field is applied. If the amount of the chiral dopant in the system is large, a cascade of intermediate "blue phases" (BP)[33]

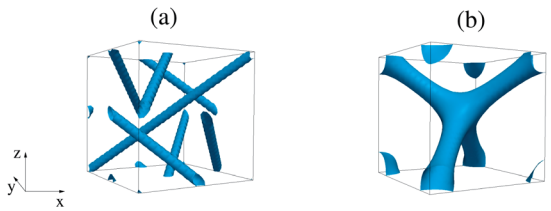

Fig. 6 Equilibrium BPI (a) and BPII (b) defect network in a cubic cell with periodic boundaries. Reproduced from ref. 27 with permission from The Royal Society of Chemistry.

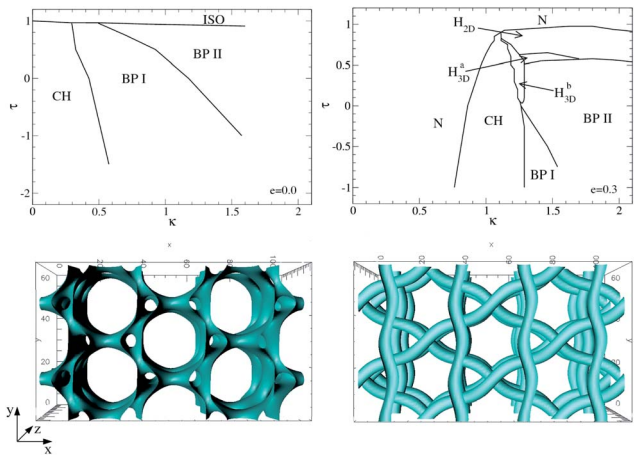

Fig. 7 Blue phase diagrams in the chirality κ–temperature τ plane without a field (top left) and for a finite field strength (top right). The bottom row depicts the two three-dimensional hexagonal blue phases H^{a}_{3D} and H^{b}_{3D}. Reproduced from ref. 43."Copyright (2010) by the American Physical Society".

can become stable between the cholesteric and the isotropic phase. The peculiar feature of blue phases is that they exhibit a fully periodic three-dimensional network of defects (see Fig. 6). As anticipated, the typical length scale of this defect network is of the order of the wavelength of visible light, which adds to their unique optical properties.

In particular BPI and BPII defects or disclinations are organised in ordered lattices with specific space symmetry groups that are associated with crystals. BPIII in contrast appears to be amorphous.[34] The periodicity of the defect structure leads to vivid scattering peaks.[35] Because of their fluidity, the optical properties of BPs are easily controlled by electric fields.[36–38] The issues related to their initially limited range of thermal stability of about 1 K that early experimentalists faced have now been resolved by means of new composite and compound media offering stability over an impressive range (up to even 200 K in width), including room temperature.[39,40] These innovations led to the recent construction of the first prototype of a blue-phase display with promisingly fast switching and response times.[41]

We discuss now some of the most recent numerical studies on the effects of applied external electric fields and hydrodynamic interactions in BPs, mainly focusing our attention on the evolution of the defect network in periodic and confined cells. The general picture that emerges from these studies is that the defect dynamics depends sensitively

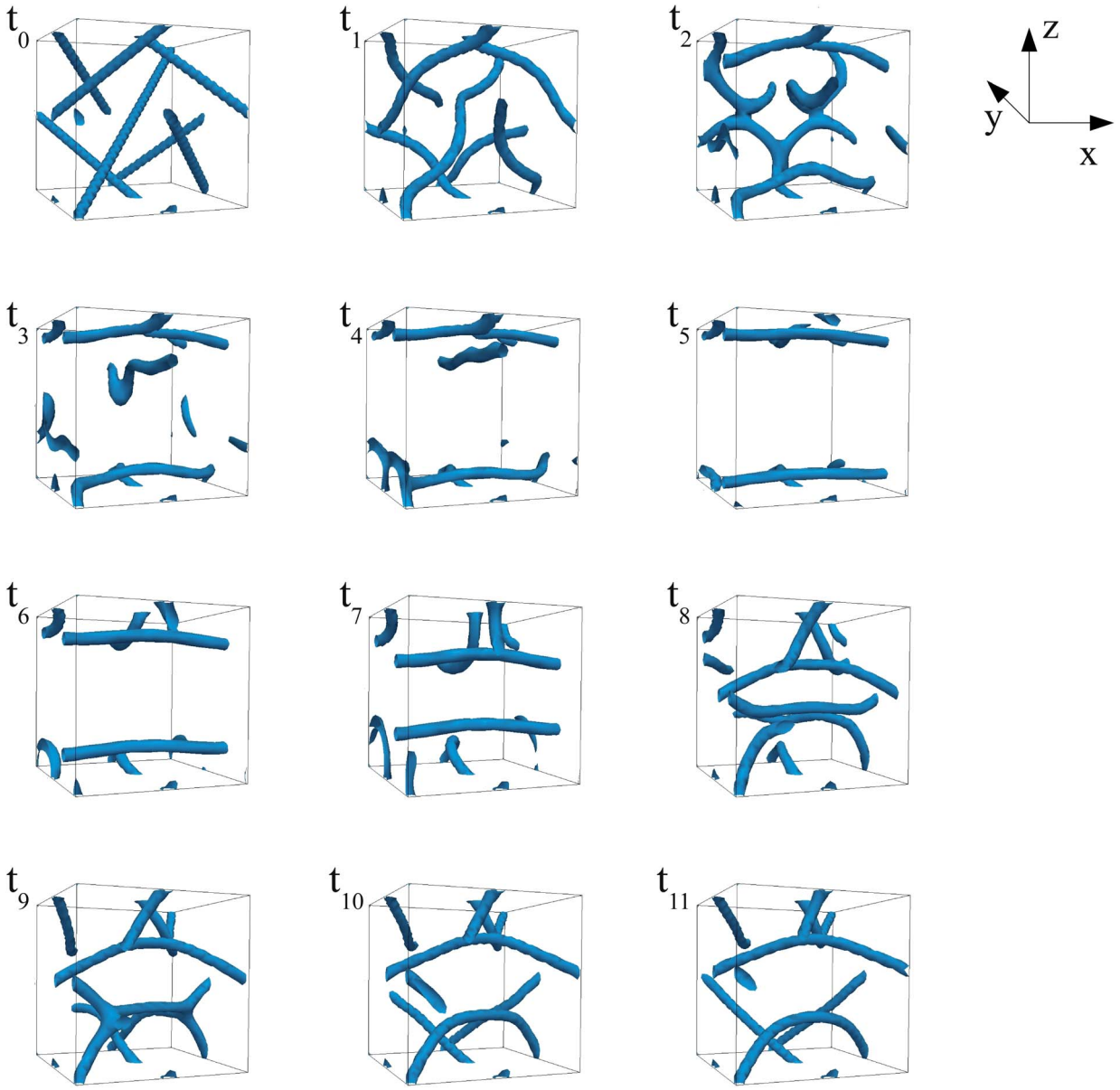

Fig. 8 Time evolution of the defect network of the BPI phase during the switching on (t_0–t_5)–off (t_6–t_{11}) dynamics in a cubic cell with an electric field applied along the z-direction ([0, 0, 1]). Strong anchoring is set on both walls. Although the final configuration (t_{11}) has a different defect structure with respect to the typical network of the BPI (t_0), after several cycles, the switching is reversible between the states t_5 and t_{11}, making the system usable as a device. Reproduced from ref. 27 with permission from The Royal Society of Chemistry.

on parameters of the applied field, and particularly on its magnitude and direction.

Before we proceed to discuss setups with specific boundary conditions, it is instructive to consider the bulk switching behaviour of blue phases. At finite field strengths and for certain thermodynamic parameters blue phases with a hexagonal spatial symmetry emerge as stable equilibrium phases. The top left image in Fig. 7 shows a blue phase diagram in the absence of external electric fields, featuring the cholesteric state and two cubic blue phases, BPI and BPII, at low temperature, as well as the isotropic state at high temperature. Note that amorphous BPIII is not depicted in this phase diagram. It would enclose the BPII region (see ref. 42 for instance). At finite field strengths the isotropic state becomes unstable as the molecules align and form a field-induced nematic state. This is also the case for cholesteric states with a comparably large pitch length or low chirality, respectively. The cholesteric and both cubic blue phases move towards larger chiralities and lower temperatures and, close to the transition line to the isotropic state, a region of stable hexagonal blue phases appears. The two bottom images in Fig. 7 give snapshots of both three-dimensional hexagonal blue phases H^{a}_{3D} and H^{b}_{3D}. The phase stability depends on all three key parameters, namely temperature, chirality or inverse pitch length, and field strength, and is rather intricate. Ultimately the topology of the underlying defect network determines the range of stability. In general the region of stability of hexagonal blue phases grows with increasing field strength at the cost of the cubic blue phases, whose range of stability is also restricted from the high-chirality end where the field-induced nematic state is energetically more favourable.

Having discussed the behaviour of bulk blue phases under an electric field, we continue by highlighting some modelling work on device designs based on blue phases. When, for example, a sufficiently strong field is applied perpendicular to the walls in a BPI cell, a complex reorganisation of the defect structure takes place. Typically disclination lines twist up during the switching on until they merge to form unstable branching points that annihilate in the bulk, creating a state with defects pinned up against the walls. When the field is removed, some arcs of the disclination lines migrate back to the centre of the cell while others join to disclinations that are situated close to the boundaries (see Fig. 8). After one such cycle the device is therefore stuck in a metastable state whose total free energy is higher than that with zero-field (in equilibrium). Starting from the last metastable state, a further application of the electric field guides the system towards the same field-induced state. This switching behaviour constitutes a reversible cycle which makes the cell suitable for use as a device (in other words, the device is "switchable" as per previous definition). As the magnitude or the direction of the field changes, several different kinetic pathways can be observed, provided the field strength is above a critical threshold, below which the topology of the equilibrium structure remains unaltered.[27]

As in nematic devices, hydrodynamic interactions play an important role in determining the kinetic pathway during the switching event. In the BPI devices studied numerically, they reduce relaxation times, speeding up the evolution towards steady states (see discussion in ref. 27). More qualitatively, the inertial coupling of the order parameter to the velocity field prevents the system from getting trapped in metastable states. This drives the system towards states with lower free energy.[27]

The switching dynamics in a BPII cubic cell is simpler, although still interesting. An intense electric field applied perpendicular to the walls breaks the defect network creating a disclination loop that afterwards splits into two disclination lines which are pinned up at the boundaries. As the field is switched off, the structure recovers its initial zero-field state, making the BPII cell a potential candidate for an electrically switchable device (see ref. 27 for more details).

An important and non-trivial question deals therefore with the choice of boundary conditions. In the previously discussed simulations the director at both walls was kept fixed at its equilibrium configuration in the absence of any field. These conditions have often been used in studies of cholesteric and blue phases,[31,44–47] although they might be difficult to realise experimentally (in practice one would require a specific patterning of surface defects to fix the topology at the boundaries). On the other hand, it is much simpler for experimentalists to control the alignment by rubbing the surface in order to obtain a homogeneous (or parallel) anchoring, or by chemical treatment to favour homeotropic (or perpendicular) anchoring. In both cases the effect of this treatment on the disclination network is known to be confined to a single cell of the order of a few micrometers.

Several recent studies have focused on BPs confined in a single cell with either homeotropic or homogeneous anchoring. It has been shown that in both cases the typical equilibrium defect network is significantly modified and several metastable states are introduced. Their structure depends mainly on the distance between the walls as well as on the anchoring strength. Some of them are similar to the equilibrium defect structures, whereas others have a totally different topology. Arrays formed of double-helix disclination lines are observed, for example, in cells with homeotropic anchoring.[48] A regular array of isolated ring defects emerges when homogeneous anchoring is

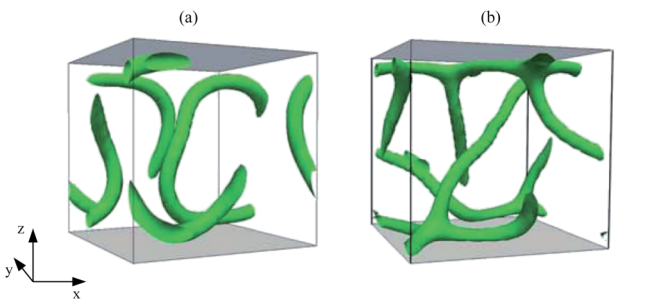

Fig. 9 Zero-field equilibrium defect network for a cubic BPI cell with (a) homogeneous and (b) homeotropic anchoring on both walls (in grey). While ring defects emerge when the director is parallel to the surface, a BPI defect-like network is observed when the director is perpendicular. More exotic topologies can be seen in ref. 48. Reproduced from ref. 55 with permission from The Royal Society of Chemistry.

considered.[49] In Fig. 9 we show some possible equilibrium defect structures obtained from simulations.

The switching hydrodynamics associated with these novel structures is far from trivial and complex patterns have been observed during an electric field induced director evolution even in the absence of hydrodynamic interactions.[50]

A key requirement to utilise BP structures in devices is to understand and control the kinetic route the system takes when moving between these electric field induced configurations. Being able to switch between different metastable configurations could in turn lead to multistable devices, which as previously discussed are of interest as energy-efficient liquid crystal technology. A successful example of this has been the theoretical identification of two bistable BP devices: the first one utilises surface memory effects that retain the BPI structure on the boundaries, whereas the second one entails homeotropic anchoring in a confined cubic cell.[51] In Fig. 10 the switching dynamics of a confined BPI cell with homeotropic anchoring on both walls is shown. The device switches between two metastable zero-field states (t_8 and t_{16}), the first of which is characterised by a double-helical arrangement of defects whereas in the second one disclinations form twisted rings.

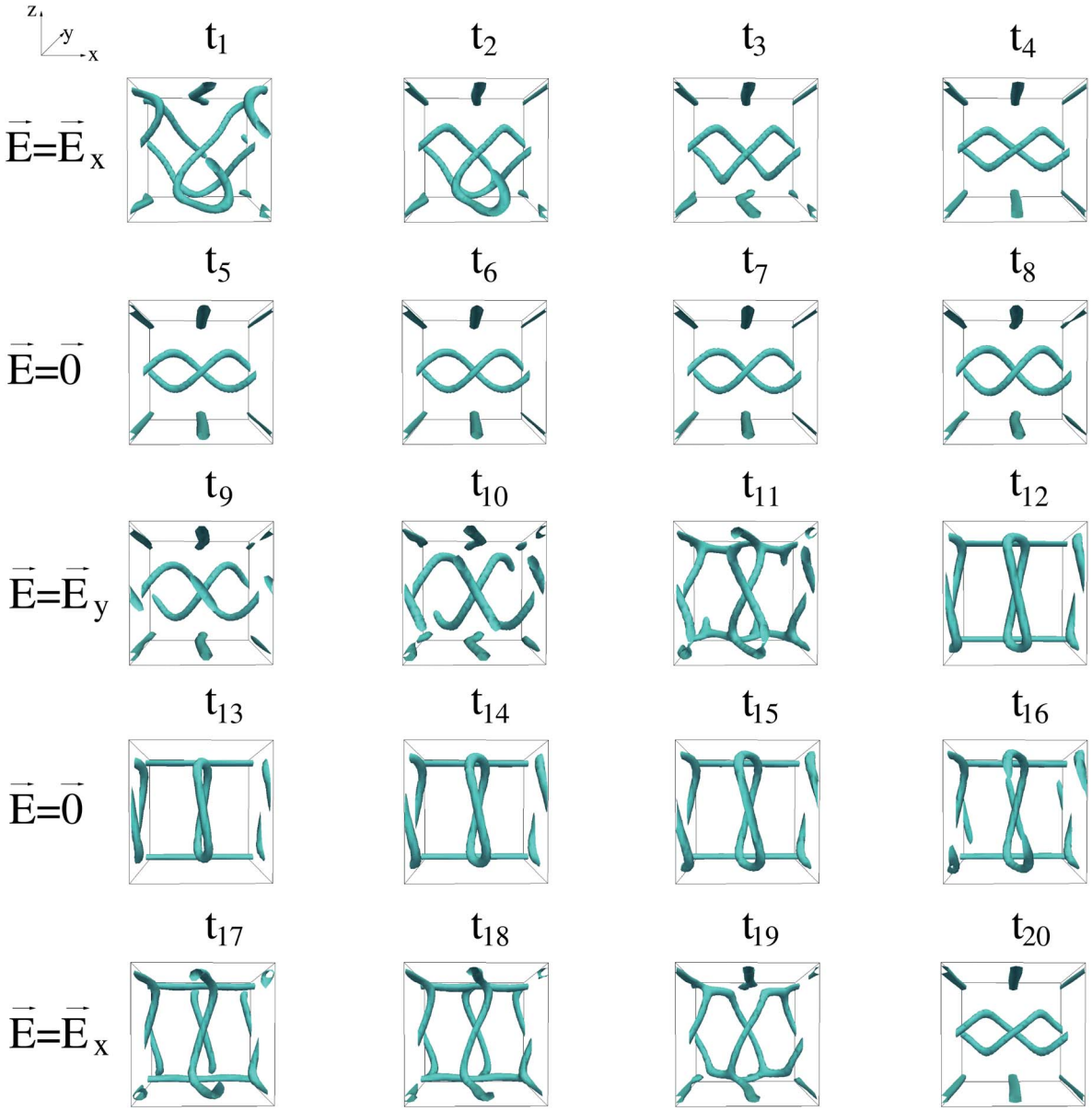

Fig. 10 Time evolution of the disclination network in the BPI bistable cell with homeotropic anchoring on both walls. An electric field is initially switched on along the *x*-direction (t_1–t_4). After a double-helical steady state is reached the field is switched-off (t_5–t_8) and the system evolves towards a zero-field state with a similar defect structure. Afterwards the field is switched on along the *y*-direction. The system is now driven towards a state characterised by twisted ring defects (t_9–t_{12}) that are unaltered after the field is removed (t_{13}–t_{16}). A further application of the field is necessary to have a bistable device. It is applied again along the *x*-direction allowing the system to recover the double-helical topology (t_{17}–t_{20}). Reproduced from ref. 51. "Copyright (2011) by the American Physical Society".

It is likewise interesting to see how the kinetic process changes during the switching when boundaries are removed and bulk behaviour is probed. This has been studied in ref. 52 where the authors show that, for BPI and BPII cells, the evolution is strongly affected by the direction and magnitude of the electric field and by the sign of the dielectric anisotropy as well. When the field is on, the authors report that the disclination network rearranges creating complicated topological textures. Later on, the system ends up in a field-induced defect-free nematic or cholesteric state. Typical switching off times in these BP-based devices are in the 0.01–0.1 ms range, in line with what is expected based on a simple estimate by using eqn (1) with the unit cell size ($\sim p$) in place of L (the switching on time varies more as it is field dependent).

A different instance of bulk switching behaviour has been studied for the case of amorphous BPIII,[34] also known as the "blue fog". Numerical simulations have suggested that the structure of the blue fog is locally similar to that of BPII (Fig. 6), but without any long-range quasi-crystalline order of the disclination network. Fig. 11 shows such a switching event starting from the amorphous BPIII network. The field-induced configuration consists of a staggered array of helical, corkscrew-like disclination lines. This ordering is consistent with a sharper peak in scattering data, which has been observed in experiments – no experimental structural data currently exist on this phase though. The lattice constant of the theoretically observed structure is different along and perpendicular to the direction of the external field, as visible in the peak structure shown in the cuts through simulated structure factor data in the bottom row of Fig. 11. It is worth mentioning that in this case there is no sign for metastability and, after the field has been switched off, the ordered state returns to an amorphous conformation equivalent to the original one. This, however, holds for bulk switching: confined samples may well possibly lead to different conclusions.

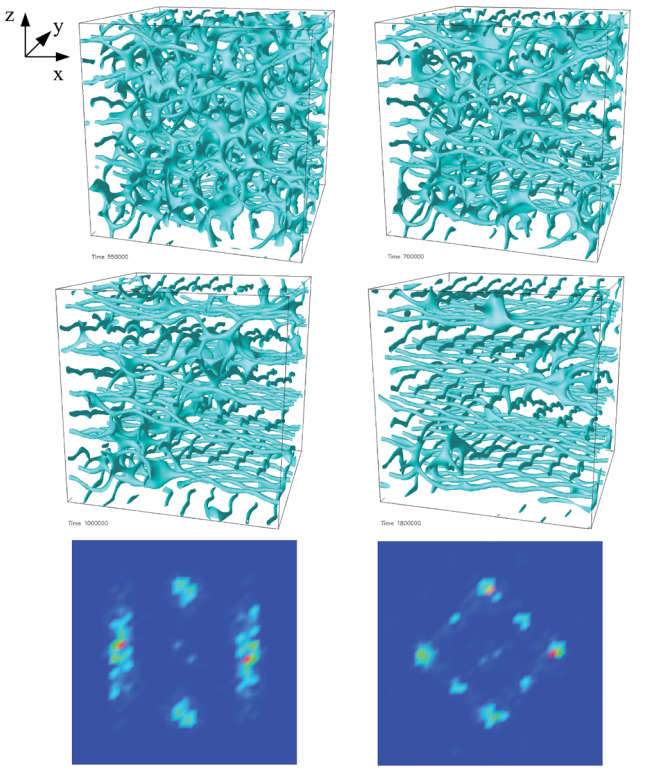

Fig. 11 Disclination network during the transition from the amorphous BPIII to a field-induced blue phase, sometimes referred to as BPE. The snapshots show approximately times $t \simeq 0.15$, 0.3, 0.6 and 1.4 ms after switching on the field. The bottom row depicts structure factor data $C(\mathbf{k})$ at the end of the run at $k_y = 0$ and $k_z = 0$, respectively. Reproduced from ref. 34."Copyright (2011) by the American Physical Society".

Before concluding it is important to recap the experimental situation. As anticipated, the technological applicability of BPs has been enormously increased by the recent discovery of polymer and temperature stabilised blue phases.[39,53] In ref. 39, in particular, the authors propose a blue phase in which disclination lines are stabilised as a consequence of high flexoelectricity – this mechanism leads to a stability range of up to 200 K! Clearly, for future applications a key research area will be the understanding of the switching dynamics of such flexoelectric blue phases; the first step in this direction has been made in the recent work in ref. 55 (for a related study where flexoelectricity leads to BP-like structures in nematics, see instead ref. 54). Similar to what has previously been seen for dielectric fields, the switching dynamics in flexoelectric materials is characterised by global rearrangement of the defect structures of BPs. In a BPI cell for example the electric field drives the system towards a state in which columnar field-aligned disclinations are organised in a hexagonal patterned structure. How this structure interacts with boundaries is currently unknown, and there are no studies of a similar pattern in a confined geometry. Such studies will be important to the design of new devices based on the switching of the newly synthesised flexoelectric BPs of ref. 39.

4 Conclusions

In this review we have presented an overview of recent computer simulation studies concerning the switching hydrodynamics within LC devices. These both highlight the richness of the physics of such devices, and also address important technological issues with device functioning. For instance, theoretical studies of multidomain devices are instrumental to the resolution of the "viewing angle" problem, whereas the simulation driven design of multistable switchable devices is relevant for producing energy-saving devices, which are required for many present-day applications such as smart glass, e-paper and portable flexible displays.

This review cannot by any means be exhaustive in describing all physical and technological aspects of devices. Hence, we discussed the physics of a selection of these, together with a brief mention of both their advantages and drawbacks. Furthermore, for reasons of space we did not include a detailed description of other interesting and important technological solutions, such as *in-plane switching* and *vertical alignment*. Likewise, we did not discuss some of the most recent advances like embedded nanoparticles in an LC matrix, a technology that finds

application in e-ink technologies. Although this represents a growing and challenging area of research, the largest part of devices that are traded today on markets are free of colloids or nanoparticles. Finally, we omitted a substantial number of other factors that affect the correct operation of LC devices, such as the colour depth and its permanence as well as the timing performance. These factors might affect the switching dynamics, although not the generic features we presented in this review.

We hope this selection of results has conveyed the message that the physics behind the working mechanisms of liquid crystal devices is extremely interesting, and that there are a number of open questions which would be worthwhile addressing in the future. Understanding the disclination dynamics is of paramount importance for the improvement of design and performance of devices. This is particularly true for systems like those based on blue phases where the complicated topological structure makes it difficult to understand the way in which a target structure can be accessed by means of a specific protocol. At the same time, defects are an inevitable consequence of the surface patterning used in many multidomain nematic devices: in these systems a loss of resolution is traded in for a larger viewing angle. Finding a fully satisfactory solution of the viewing angle problem that avoids the drawback of creating defects is currently still a challenge. Another fundamental and open question deals with reduced power consumption of LC devices. Many efforts have been made since the 1980s with some outstanding achievements such as the zenithal bistable device which uses nematics[17–19] and surface stabilised cholesteric textures.[32] Most of these technologies rely on bistable or multistable behaviour. New possibilities have been opened up when blue phases were discovered to be stable over a wide temperature range. The plethora of competing metastable states arising in blue phase systems arguably represents promising potential for achieving multistability, provided the kinetic pathway for a reversible switching is accessible. An example of an experimentally realised bistable BP does exist, and is demonstrated in ref. 56. However, its technological feasibility remains unexplored. The use of flexoelectric effects could provide another route to lower the energy footprint of devices. Denniston *et al.* proposed a flexoelectric surface switching mechanism,[17] which is responsible for bistable behaviour in a nematic device.[18] More recently simulations revealed the possibility of using a surface flexoelectric field to dynamically control the switching of a blue phase cell.

Overall, we feel therefore that there is still a lot of physics to be discovered lurking behind the functioning of liquid crystal devices, and this will surely assist new creative and innovative technologies by revealing fundamental principles.

Appendix

Here, for completeness, we briefly review one of the main physical models used to study liquid crystal hydrodynamics. This is a continuum model (often termed Beris–Edwards[20]) in which hydrodynamic interactions are consistently taken into account to describe non-chiral liquid crystals and, in a more generalised form, chiral liquid crystals. We note that this hydrodynamic theory is suitable to describe the dynamics of liquid crystal devices,[57] for which switching times are 0.1 ms or above.

The local order of a liquid crystal can be described in terms of a tensorial order parameter $\mathbf{Q}$, which is in turn related to the local direction of individual molecules $\hat{\mathbf{n}}$ by $Q_{\alpha\beta} = \left\langle \hat{n}_\alpha \hat{n}_\beta - \frac{1}{3}\delta_{\alpha\beta} \right\rangle$, where the angular bracket denotes a coarse-grained average, the Greek indices label the Cartesian components of $Q_{\alpha\beta}$ and $\delta_{\alpha\beta}$ is the unit matrix. The tensor $Q_{\alpha\beta}$ is traceless and symmetric and its largest eigenvalue, $2/3q$ $(0 < q < 1)$, measures the magnitude of local order.

Equilibrium properties are encoded in a free energy density f[1,20,33] written on the basis of the characteristic symmetries of the system, and considering high enough order terms to describe a phase transition. The free energy comprises a bulk term (which is the sum of only rotational invariants of the form $Q_{\alpha\beta}{}^p$ with $p \in \{2, 3, \ldots\}$)

$$f_b = \frac{A_0}{2}\left(1 - \frac{\gamma}{3}\right) Q_{\alpha\beta}{}^2 + \frac{A_0\gamma}{3} Q_{\alpha\beta} Q_{\beta\gamma} Q_{\gamma\alpha} + \frac{A_0\gamma}{4}\left(Q_{\alpha\beta}{}^2\right)^2, \qquad (3)$$

and an elastic term which is

$$f_{el} = \frac{K}{2}\left(\partial_\beta Q_{\alpha\beta}\right)^2 + \frac{K}{2}\left(\varepsilon_{\alpha\zeta\delta}\partial_\zeta Q_{\delta\beta} + \frac{4\pi}{p_0} Q_{\alpha\beta}\right)^2. \qquad (4)$$

The bulk free energy describes the transition from the isotropic to the liquid crystal phase and the elastic contribution takes into account the energy cost due to the presence of the typical bulk distortions, namely splay, bend and twist. In the former formula A_0 is a constant (with units of pressure) and γ plays the role of an effective temperature or concentration according to whether thermotropic or lyotropic liquid crystals are considered. In the latter one, K is the elastic constant (in the one-constant approximation), $\varepsilon_{\alpha\zeta\delta}$ is the Levi-Civita antisymmetric third-rank tensor and p_0 is the intrinsic helix pitch of the cholesteric. In the nematic limit (in which the pitch is very large) the second term of eqn (4) turns out to be zero.

The coupling of an external electric field E_α to a liquid crystal occurs in two forms, namely the dielectric one, in which it is linear to the order parameter $\mathbf{Q}$ and quadratic with the electric field, and the flexoelectric one, in which it is now linear in the electric field and quadratic in the order parameter. To account for the former, we add the following term to the free energy density[1]

$$f_{diel} = -\frac{\varepsilon_a}{12\pi} E_\alpha Q_{\alpha\beta} E_\beta, \qquad (5)$$

where ε_a is the dielectric anisotropy of the liquid crystal. The flexoelectric contribution is instead given by[54]

$$f_{flexo} = \varepsilon_{fl}^b Q_{\alpha\beta}(E_\alpha \partial_\gamma - E_\gamma \partial_\alpha) Q_{\beta\gamma}, \qquad (6)$$

where ε_{fl}^b is the bulk flexoelectric constant. The dielectric coupling is typical of rod-like molecules: when the field is on, these tend to align parallel or perpendicular to the field itself, depending on the sign of the dielectric anisotropy. Conversely, the flexoelectric coupling occurs with pear- or banana-shaped molecules, in which an elastic distortion

determines a spontaneous polarisation. On the other hand polarisation can be induced by an external field, giving rise to an elastic distortion.

The last contribution to the free energy is the surface one, given by

$$f_s = \frac{W_0}{2}\left(Q_{\alpha\gamma} - Q^0_{\alpha\gamma}\right)^2 + \frac{K}{2}\left[\left(\partial_\alpha Q_{\beta\gamma}\right)^2 + \left(\partial_\alpha Q_{\alpha\gamma}\right)\left(\partial_\beta Q_{\beta\gamma}\right)\right] + \varepsilon^s_{fl}\left(\partial_\beta Q_{\alpha\beta}\right)E_\alpha, \quad (7)$$

with $Q^0_{\alpha\beta} = S_0(n^0_\alpha n^0_\beta - \delta_{\alpha\beta}/3)$ and S_0 determining the magnitude of surface order. The first term of eqn (7) is a quadratic contribution ensuring a soft pinning of the director field on the boundary surface to a chosen direction $\hat{n}_0$. The parameter W_0 controls the strength of the anchoring and it is practically infinite in the strong anchoring regime, in which the director field is effectively fixed at the boundaries. The second term is necessary in the weak anchoring regime where elastic distortions at the surfaces need to be included. Finally, the third term is a flexoelectric contribution at the boundary surfaces (multiplied ε^s_{fl} which is the surface flexoelectric constant) which depends linearly on the gradients of **Q** and is irrelevant in the strong anchoring regime.[55]

The equation of motion for **Q** is[20]

$$(\partial_t + \vec{u}\cdot\nabla)\mathbf{Q} - \mathbf{S}(\mathbf{W}, \mathbf{Q}) = \Gamma\mathbf{H} \quad (8)$$

where Γ is a collective rotational diffusion constant, which is related to the rotational viscosity, γ_1. The left hand side of eqn (8) is the material derivative which is constituted of two terms: the first one takes into account the time dependence from advection by a fluid with velocity $\vec{u}$, and the second one $\mathbf{S}(\mathbf{W}, \mathbf{Q})$ describes the fact that the order parameter distribution can be rotated and stretched by the fluid. This term depends on the gradient velocity tensor $W_{\alpha\beta} = \partial_\beta u_\alpha$ and is given by

$$\mathbf{S}(\mathbf{W}, \mathbf{Q}) = (\xi\mathbf{D} + \boldsymbol{\omega})(\mathbf{Q} + \mathbf{I}/3) + (\mathbf{Q} + \mathbf{I}/3)(\xi\mathbf{D} - \boldsymbol{\omega}) - 2\xi(\mathbf{Q} + \mathbf{I}/3)T_r(\mathbf{QW}) \quad (9)$$

where T_r denotes the tensorial trace and $\mathbf{D} = (\mathbf{W} + \mathbf{W}^T)/2$ and $\boldsymbol{\omega} = (\mathbf{W} - \mathbf{W}^T)/2$ are the symmetric and the anti-symmetric part of the velocity gradient tensor $W_{\alpha\beta}$. The constant ξ depends on the aspect ratio of the molecules of the liquid crystal and controls the response of the director field in a shear flow. This can be flow-aligning (large ξ), in which molecules form a fixed angle with respect to the flow direction (Leslie angle), or flow tumbling (small ξ) where they continuously change their orientation in a chaotic way. The right-hand side of eqn (8) describes the relaxation of the order parameter towards an equilibrium state, process guided by the molecular field **H** which is obtained by taking the symmetric and traceless part of the functional derivative of the free energy $\mathscr{F} = \int \mathrm{d}V f$ with respect to the order parameter **Q**

$$\mathbf{H} = -\frac{\delta\mathscr{F}}{\delta\mathbf{Q}} + (I/3)T_r\frac{\delta\mathscr{F}}{\delta\mathbf{Q}}, \quad (10)$$

with **I** being the unit matrix.

The equation for the fluid density ρ is the continuity equation

$$\partial_t\rho + \partial_\alpha(\rho u_\alpha) = 0, \quad (11)$$

which becomes $\partial_\alpha u_\alpha = 0$ in the incompressible limit. In this approximation the Navier–Stokes equation describing the evolution of the fluid velocity is

$$\rho(\partial_t + u_\beta\partial_\beta)u_\alpha = \eta\partial_\beta(\partial_\alpha u_\beta + \partial_\beta u_\alpha) + \partial_\beta(\Pi_{\alpha\beta}), \quad (12)$$

where η is an isotropic viscosity and $\Pi_{\alpha\beta}$ is the liquid crystal stress tensor, whose detailed full expression is

$$\Pi_{\alpha\beta} = -P_0\delta_{\alpha\beta} + 2\xi\left(Q_{\alpha\beta} + \frac{1}{3}\delta_{\alpha\beta}\right)Q_{\gamma\varepsilon}H_{\gamma\varepsilon} - \xi H_{\alpha\gamma}\left(Q_{\gamma\beta} + \frac{1}{3}\delta_{\gamma\beta}\right) - \xi\left(Q_{\alpha\gamma} + \frac{1}{3}\delta_{\alpha\gamma}\right)H_{\gamma\beta} - \partial_\alpha Q_{\gamma\nu}\frac{\partial f}{\partial\partial_\beta Q_{\gamma\nu}} + Q_{\alpha\gamma}H_{\gamma\beta} - H_{\alpha\gamma}Q_{\gamma\beta}. \quad (13)$$

In the case of a simple fluid $\Pi_{\alpha\beta} = -P\delta_{\alpha\beta}$, where P is the isotropic pressure, whereas in the case of a liquid crystal it describes the elastic stress exerted by molecules on the fluid due to local deformations in the director field. It is important to note that, unless the flow field is zero ($\vec{u} = 0$), the dynamics of the order parameter are not purely relaxational. The order parameter field affects the dynamics of the flow field through the stress tensor, which depends on the molecular field **H** and on **Q**. This is called backflow coupling and it needs to be properly taken into account when hydrodynamic interactions are included. The lattice Boltzmann simulations reviewed in the main text are ideally placed to do so.[21]

Acknowledgements

We thank EPSRC for funding under grant no. EP/J007404. OH acknowledges support from the Centre for Numerical Algorithms and Intelligent Software (NAIS).

References

1 P. G. de Gennes and J. Prost, *The Physics of Liquid Crystals*, Clarendon Press, Oxford, 2nd edn, 1993.
2 K.-H. Kim and J.-K. Song, *NPG Asia Mater.*, 2009, **1**, 29.
3 *Liquid Crystal Applications and Uses*, ed. B. Bahadur, World Scientific, Singapore, 1990, vol. 1.
4 J. P. F. Lagerwall and G. Scalia, *Curr. Appl. Phys.*, 2012, **12**, 1387.
5 M. Warner and E. M. Terentjev, *Liquid Crystal Elastomers (International Series of Monographs on Physics)*, Oxford University Press, USA, 2007.
6 M. Ravnik, G. P. Alexander, J. M. Yeomans and S. Zumer, *Proc. Natl. Acad. Sci. U. S. A.*, 2011, **108**, 5188.
7 P. Spicer, *Curr. Opin. Colloid Interface Sci.*, 2005, **10**, 274.
8 R. Mezzenga, P. Schurtenberger, A. Burbidge and M. Michel, *Nat. Mater.*, 2005, **4**, 729.
9 M. C. Marchetti, J. F. Joanny, S. Ramaswamy, T. B. Liverpool, J. Prost, M. Rao and R. Aditi Simha, *Rev. Mod. Phys.*, 2013, **85**, 1143.

10 H. P. Zhang, A. Be'er, E.-L. Florin and H. L. Swinney, *Proc. Natl. Acad. Sci. U. S. A.*, 2010, **107**, 13626.
11 R. Aditi Simha and S. Ramaswamy, *Phys. Rev. Lett.*, 2002, **89**, 058101.
12 J. Toner and Y. Tu, *Phys. Rev. Lett.*, 1995, **75**, 4326.
13 M. Schadt and W. Helfrich, *Appl. Phys. Lett.*, 1971, **18**, 127.
14 T. J. Scheffer and J. Nehring, *Appl. Phys. Lett.*, 1984, **45**, 1021.
15 D. Marenduzzo, E. Orlandini and J. M. Yeomans, *Europhys. Lett.*, 2005, **71**, 604.
16 A. Tiribocchi, G. Gonnella, D. Marenduzzo and E. Orlandini, *Appl. Phys. Lett.*, 2010, **97**, 143505.
17 C. Denniston and J. M. Yeomans, *Phys. Rev. Lett.*, 2001, **87**, 275505.
18 L. A. Parry-Jones and S. J. Elston, *J. Appl. Phys.*, 2005, **97**, 093515.
19 A. J. Davidson and N. J. Mottram, *Phys. Rev. E: Stat., Nonlinear, Soft Matter Phys.*, 2002, **65**, 051710.
20 A. N. Beris and B. J. Edwards, *Thermodynamics of Flowing Systems*, Oxford University Press, Oxford, 1994.
21 M. E. Cates, O. Henrich, D. Marenduzzo and K. Stratford, *Soft Matter*, 2009, **5**, 3791.
22 F. Bougrioua, W. Oepts, H. de Vleeschouwer, E. Alexander, K. Neyts and H. Pauwels, *Jpn. J. Appl. Phys.*, 2002, **41**, 5676.
23 A. Lien, H. Takano, S. Suzuki and H. Uchlda, *Mol. Cryst. Liq. Cryst.*, 1991, **198**, 37.
24 M. Reichenstein, H. Stark, J. Stelzer and H. R. Trebin, *Phys. Rev. E: Stat., Nonlinear, Soft Matter Phys.*, 2002, **65**, 011709.
25 J. Kim, M. Yoneya and H. Yokoyama, *Nature*, 2002, **420**, 159.
26 J. F. Stromer, D. Marenduzzo, C. V. Brown, J. M. Yeomans and E. P. Raynes, *J. Appl. Phys.*, 2006, **99**, 064911.
27 A. Tiribocchi, G. Gonnella, D. Marenduzzo and E. Orlandini, *Soft Matter*, 2011, **7**, 3295.
28 J. Chen, P. J. Bos, D. R. Bryant, D. L. Johnson, S. H. Jamal and J. R. Kelly, *Appl. Phys. Lett.*, 1995, **67**, 1990; J. Chen, P. J. Bos, D. L. Johnson, D. R. Bryant, J. Li, S. H. Jamal and J. R. Kelly, *J. Appl. Phys.*, 1996, **80**, 1985.
29 J. G. Cuennet, A. E. Vasdekis, L. De Sio and D. Psaltis, *Nat. Photonics*, 2011, **5**, 234.
30 O. Henrich, K. Stratford, P. V. Coveney, M. E. Cates and D. Marenduzzo, *Soft Matter*, 2013, **9**, 10243.
31 O. Henrich, K. Stratford, D. Marenduzzo, P. V. Coveney and M. E. Cates, *J. Phys.: Condens. Matter*, 2013, **24**, 284127.
32 D.-K. Yang, X.-Y. Huang and Y.-M. Zhu, *Annu. Rev. Mater. Res.*, 1997, **27**, 117.
33 D. C. Wright and N. D. Mermin, *Rev. Mod. Phys.*, 1989, **61**, 385.
34 O. Henrich, K. Stratford, M. E. Cates and D. Marenduzzo, *Phys. Rev. Lett.*, 2011, **106**, 107801.
35 H. Stegemeyer, T. H. Blümel, K. Hiltrop, H. Onusseit and F. Porsch, *Liq. Cryst.*, 1986, **1**, 3.
36 V. E. Dmitrenko, *Liq. Cryst.*, 1989, **5**, 847.
37 G. Heppke, B. Jerome, H.-S. Kizerow and P. Pieranski, *J. Phys.*, 1991, **50**, 2991.
38 P. Etchegoin, *Phys. Rev. E: Stat., Nonlinear, Soft Matter Phys.*, 2000, **62**, 1435.
39 H. J. Coles and M. N. Pivnenko, *Nature*, 2005, **436**, 997.
40 F. Castles, F. V. Day, S. M. Morris, D.-H. Ko, D. J. Gardiner, M. M. Qasim, S. Nosheen, P. J. W. Hands, S. S. Choi, R. H. Friend and H. J. Coles, *Nat. Mater.*, 2012, **11**, 599.
41 http://www.physorg.com/news129997960.html, 2008.
42 D. K. Yang and P. P. Crooker, *Phys. Rev. A*, 1987, **35**, 4419.
43 O. Henrich, D. Marenduzzo, K. Stratford and M. E. Cates, *Phys. Rev. E: Stat., Nonlinear, Soft Matter Phys.*, 2010, **81**, 031706.
44 W. Helfrich, *Phys. Rev. Lett.*, 1969, **23**, 372.
45 T. C. Lubenski, *Phys. Rev. A: At., Mol., Opt. Phys.*, 1972, **6**, 452.
46 D. Marenduzzo, E. Orlandini and J. M. Yeomans, *Phys. Rev. Lett.*, 2004, **92**, 188301.
47 A. Dupuis, D. Marenduzzo, E. Orlandini and J. M. Yeomans, *Phys. Rev. Lett.*, 2005, **95**, 097801.
48 J. Fukuda and S. Zumer, *Phys. Rev. Lett.*, 2010, **104**, 017801.
49 J. Fukuda and S. Zumer, *Phys. Rev. Lett.*, 2011, **106**, 097801.
50 J. Fukuda and S. Zumer, *Phys. Rev. E: Stat., Nonlinear, Soft Matter Phys.*, 2013, **87**, 042506.
51 A. Tiribocchi, G. Gonnella, D. Marenduzzo, E. Orlandini and F. Salvadore, *Phys. Rev. Lett.*, 2011, **107**, 237803.
52 J. Fukuda, M. Yoneya and H. Yokoyama, *Phys. Rev. E: Stat., Nonlinear, Soft Matter Phys.*, 2009, **80**, 031706.
53 H. Kikuchi, M. Yokota, Y. Hisakado, H. Yang and T. Kajiyama, *Nat. Mater.*, 2002, **1**, 64–68.
54 G. P. Alexander and J. M. Yeomans, *Phys. Rev. Lett.*, 2007, **99**, 067801.
55 A. Tiribocchi, M. E. Cates, G. Gonnella, D. Marenduzzo and E. Orlandini, *Soft Matter*, 2013, **9**, 4831.
56 C.-T. Wang, H.-Y. Liu, H.-H. Cheng and T.-H. Lin, *Appl. Phys. Lett.*, 2010, **96**, 041106.
57 S. Chandrasekhar, *Liquid Crystals*, Cambridge University Press, Cambridge, 1992.

